JOURNAL OF GEOPHYSICAL RESEARCH, VOL. 114, A07304, doi:10.1029/2009JA014057, 2009

Characterizing the 10 November 2004 storm-time middle-latitude plasma bubble event in Southeast Asia using multi-instrument observations

Guozhu Li,[1,2] Baiqi Ning,[1] Biqiang Zhao,[1] Libo Liu,[1] Weixing Wan,[1] Feng Ding,[1] J. S. Xu,[3] J. Y. Liu,[4] and K. Yumoto[5]

Received 7 January 2009; revised 9 March 2009; accepted 18 March 2009; published 7 July 2009.

[1] The development and dynamics of ionospheric plasma bubble (PB) irregularity during the super storm of 7–11 November 2004 are investigated using the data from a multi-instrument network operated in Southeast Asia. Analysis of fluctuations in Global Positioning System total electron content (GPS TEC), ionosonde, GPS scintillation, and in situ satellite density data indicates a series of intense PB-associated irregularities at equatorial, low, and middle latitudes in the Japanese longitude on 10 November. However, in the Chinese sector, the scintillations and PB irregularities are confined within the range of 20–50°N in geographic latitude and 110–125°E in geographic longitude. The absence of equatorial PB irregularities in this sector shows a major difference from that in the close-by longitude Japanese sector. In the Southern Hemisphere Australian sector, the irregularities occurrence is present as a symmetrical distribution at conjugate latitudes. Combined analysis of the data from Osan and Wuhan ionosondes illustrates that the middle-latitude spread *F* irregularities initially develop at the lower part of the *F* region and then distribute in the whole *F* region. This initiation of spread *F* at lower altitudes indicates that the middle-latitude PB-associated irregularities are locally generated. These results together with the irregularities occurrence sequence from higher to lower latitudes, and the onset time delay of several hours implies that the presence of PB-associated irregularities within a latitude range of 20–50°N in the Chinese sector cannot be attributed to the effects of prompt penetration electric fields (PPEFs), although the equatorial PBs in the close-by longitude are seen to be associated with PPEFs. The possible mechanism is the *F* region plasma instabilities triggered by wave structures, which act as an external driving force and seed active plasma dynamics and instability growth at middle latitude.

Citation: Li, G., B. Ning, B. Zhao, L. Liu, W. Wan, F. Ding, J. S. Xu, J. Y. Liu, and K. Yumoto (2009), Characterizing the 10 November 2004 storm-time middle-latitude plasma bubble event in Southeast Asia using multi-instrument observations, *J. Geophys. Res.*, *114*, A07304, doi:10.1029/2009JA014057.

1. Introduction

[2] Plasma bubbles (PBs) refer to irregular plasma density depletions, and have been extensively studied through a variety of observations of the *F* region ionosphere over equatorial to low and middle latitudes, such as range spread echoes from ionosonde [*Woodman and LaHoz*, 1976], rapid amplitude or phase fluctuations for the radio wave communication [e.g., *Basu et al.*, 1985; *Aarons*, 1993; *Bhattacharyya et al.*, 2001], pronounced density depletions from airglow and in situ satellites [*Kelley et al.*, 2002; *Burke et al.*, 2004; *Su et al.*, 2006], and on the basis of their signatures in the magnetic field [*Stolle et al.*, 2006]. At equatorial and low latitudes, the PBs are generally thought to be resulted from multistep nonlocal plasma processes initiated from the large-scale gravitation Rayleigh-Taylor (R-T) instability in the bottom-side ionosphere after sunset when some seeding perturbations exist (see *Keskinen et al.* [1980] and G. Haerendel, Theory of equatorial spread *F*, preprint, Max-Planck Institute for Physics and Astrophysics, Garching, Germany, 1974).

[3] The growth rate of the R-T instability depends on the external driving forces such as neutral wind [*Rama Rao et al.*, 1997], electric and magnetic fields, together with background ionospheric properties for example the flux tube integrated Pedersen conductivity and upward plasma density gradients [*Sultan*, 1996]. For the PBs and associated irregularities at middle latitude, one type is identified as the

[1]Beijing National Observatory of Space Environment, Institute of Geology and Geophysics, Chinese Academy of Sciences, Beijing, China.
[2]Also at State Key Laboratory of Space Weather, Chinese Academy of Sciences, Beijing, China.
[3]School of Electronic Information, Wuhan University, Wuhan, China.
[4]Institute of Space Science, National Central University, Chung-Li, Taiwan.
[5]Space Environment Research Center, Graduate School of Sciences, Kyushu University, Fukuoka, Japan.

0148-0227/09/2009JA014057$09.00

extension of equatorial irregularities since an equatorial plasma bubble (PB) can rise to a high apex height and extend to higher latitudes along the magnetic field line [*Huang et al.*, 2007]. Another is the local generated irregularities at middle latitude, which have been explained with the Perkins instability [*Perkins*, 1973]. Moreover, many recent papers on the instabilities of the sporadic *E* layers indicate that the electrodynamically coupled *E* and *F* regions will produce *F* region structure more rapidly than by the Perkins instability solely [*Cosgrove and Tsunoda*, 2003; *Tsunoda et al.*, 2004]. Large waves at the bottom side of the nighttime ionosphere may be one of the critical precursors that initiate the development of PB-associated irregularities at equatorial [*Hysell*, 2000] and middle latitudes [*Earle et al.*, 2006, 2008; *Xiao et al.*, 2007].

[4] Although many aspects of PBs and associated irregularities producing ionospheric scintillation have been reasonably explained on the basis of the investigations, storm-time variability of irregularities is not yet to be understood comprehensively. During storm periods, the prompt equatorward penetration of magnetospheric or high-latitude electric fields, and the ionospheric disturbance dynamo alter significantly the ionospheric electric fields in the equatorial and low-latitude regions [*Schunk and Sojka*, 1996; *Abdu*, 1997; *Liu et al.*, 2004]. Also, the transport of energy from high latitude in form of changes in global wind pattern and traveling atmospheric disturbances (TADs) owing to Joule heating or Lorentz forces can cause ionospheric perturbations [*Ding et al.*, 2007; *Lei et al.*, 2008; *Zhao et al.*, 2008]. As a result, the generation of PBs and associated irregularities in postsunset hours may be assisted or suppressed, depending on the variations of magnetospheric and ionospheric parameters which affect the strength of disturbed time instability growth rate [*Martinis et al.*, 2005]. Some recent studies have focused on the evolution of PB irregularities under storm-time conditions [e.g., *Sahai et al.*, 1994; *Basu et al.*, 2001; *Lee et al.*, 2002; *Su et al.*, 2002; *Kil et al.*, 2006]. For example, *Abdu et al.* [2003] studied the evolution of equatorial PBs and found that the disturbance dynamo plays an important role in bubble development during the storm of 26 August 1998 in the Brazilian sector. The westward PB irregularity could arise from prompt penetration disturbance zonal electric field in the course of a disturbance sequence lasting several hours. *Ma and Maruyama* [2006] presented the observations of a PB at middle latitude detected by a dense GPS TEC network in Japan, and suggested that a prompt penetrating magnetospheric electric field helped to trigger the super bubble. On the basis of multi-instrument observations at middle latitude in the Japanese sector, *Sahai et al.* [2001] found the small-scale intensity depletion structures (with scale size of 30–50 km) are caused by possible nonlinear interaction between the mesoscale traveling ionospheric disturbances (TIDs) and enhanced regions of the equatorial ionospheric anomaly, the enhanced ionospheric disturbances were confined at middle latitude during the storm of 12 February 2000.

[5] During the early part of November 2004, two long-lasting coronal mass ejections (CMEs) passed the Earth and produced a rare super double magnetic storm [*Balan et al.*, 2008]. The first super storm with a storm sudden commencement at 02:57 UT and storm main phase (MP) onset at 2130 UT on 7 November; *Dst* reached −373 nT at 0700 UT and *Kp* reached 9 during 0300–0900 UT on 8 November. While the storm was recovering, the next CME clouds during 9–12 November re-intensified the storm, with the second MP onset at 1200 UT on 9 November; *Dst* reached −289 nT at 1100 UT and *Kp* reached 9 during 0900–1200 UT on 10 November. The IMF *Bz* component, *AE*, *Kp* and *Dst* indices are shown in Figure 1. Several other workers have investigated the response of the ionosphere to this super storm [e.g., *Afraimovich et al.*, 2006; *Maruyama*, 2006; *Fejer et al.*, 2007; *Pirog et al.*, 2007; *Xu et al.*, 2007]. For example *Sahai et al.* [2009a] investigated the generation and suppression of equatorial ionospheric irregularities and the changes in the daytime *F* region electron density in the Latin American sector. This study is motivated by the interesting observations reported by *Sahai et al.* [2009b]. Using ionosonde observations at Ho Chi Minh City (Vietnam) and Okinawa, Yamagawa, Kokubunji, and Wakkanai (Japan), they found that intense spread *F* was observed at the Japanese ionospheric sounding network, but no spread *F* was observed at HCM (having a local time difference with the Japanese sector of two hours). The main purpose of the study is to utilize multi-instrument observations of Southeast Asia to help investigate the evolution and dynamics of the storm-time PB-associated irregularities, present and discuss irregularities occurrence range and associated mechanism triggering the instability. In the following sections, we first present the data sets, the observations from ground-based GPS TEC receivers, space-borne satellites, scintillation receivers and ionosondes are used to reveal the characteristics of PB events. We then proceed with a discussion of the possible mechanism responsible for the observed PB-associated irregularities. The main finding of the study is given in the Summary section.

2. Description of Data Sets

[6] Data from different ground-based and spaced-based instrumentations were used to study the response of ionosphere to intense storm of 10 November 2004. The most important information comes from the ground-based TEC measurements at sites located in Southeast Asia. As shown in Figure 2, the triangles represent the location of selected GPS TEC receivers. The rate of TEC index (ROTI) [*Pi et al.*, 1997] is obtained by converting the line-of-sight TEC to vertical TEC by assuming a thin shell ionosphere at 400 km. Using the difference of day time ROTI (R_{day}) and evening time ROTI (R_{ev}) and the threshold value of 0.075 TEC units per minute (TECu/min) as *Nishioka et al.* [2008] proposed, we examined the occurrence rates of PBs. In the following sections, ROTI means the difference value of $R_{ev} - R_{day}$. Within a square grid of 1° in geographic longitude and latitude, the number of ROTI $\geq$ 0.075 is divided by the total number of ROTI to obtain the PB occurrence rate in that square area at premidnight and postmidnight, and then obtain the grid map of PB occurrence rates. As such, the network of GPS TEC stations is an ideal platform for tracking the occurrence of the ionospheric irregularities.

[7] Another set of data is from scintillation observations, provided by ionospheric scintillation monitors (ISMs). The ISMs are based on Novatel single-frequency (L1) receivers which have been modified to process raw data sampled at 50 Hz and calculate amplitude and phase parameters which

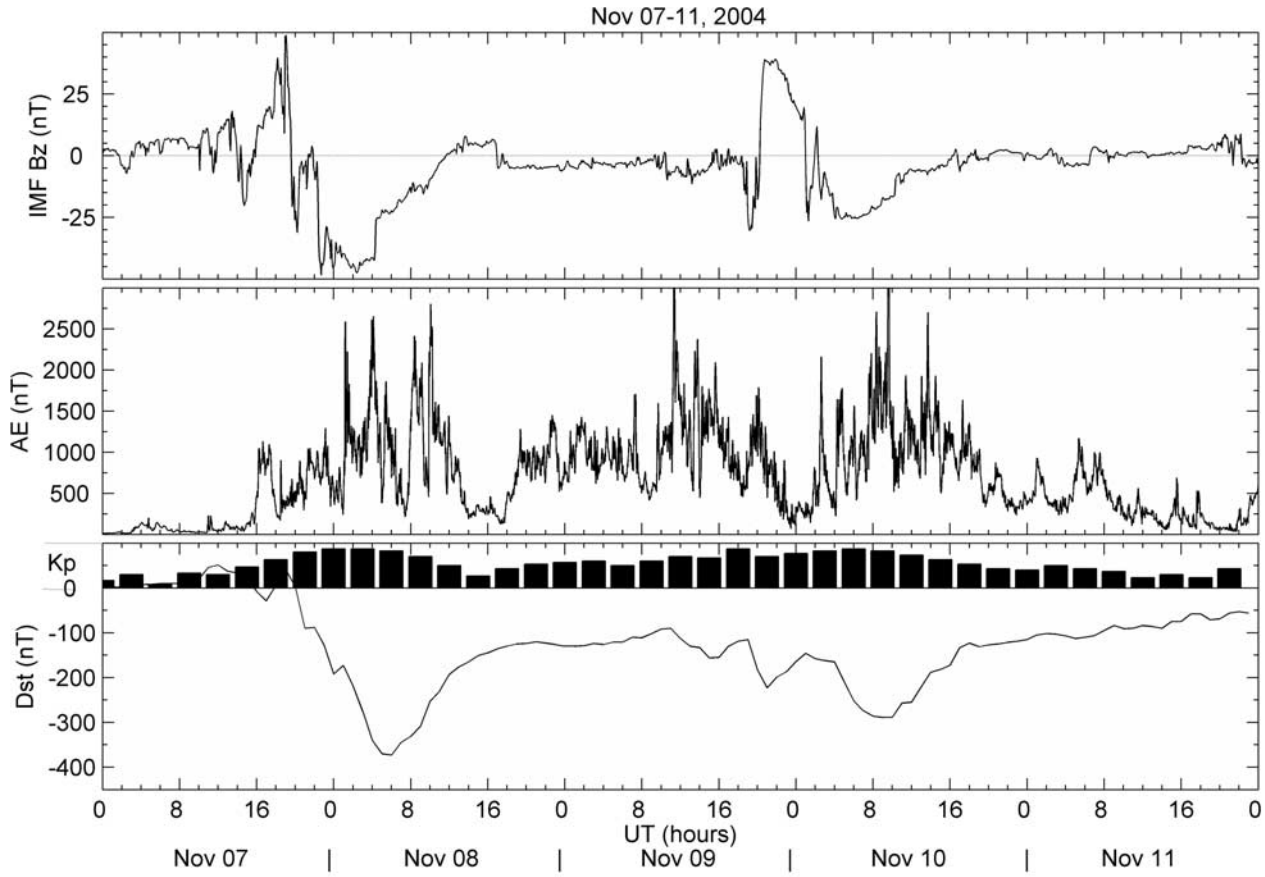

Figure 1. IMF *Bz*, *AE*, *Kp*, and *Dst* indices on 7–11 November 2004.

characterize the observed scintillation [*Van Dierendonck et al.*, 1993]. The ISMs are stationed at Wuhan and Sanya. To provide detailed information of the irregularity producing scintillation, we use the ionograms from Osan, Wuhan and Chungli ionosondes to detect the diffused *F* layer echo traces, called spread *F* irregularities. Ionograms are available at intervals of 15 min. The occurrence of range and frequency type spread *F* on these ionograms was analyzed. The information of stations (including scintillation, ionosonde and magnetometer) are listed in Table 1.

[8] Besides the ground-based observations, the space-borne satellite measurements have offered the ability to study the irregularity in different altitude of the ionosphere. The DMSP and CHAMP satellites made several passes over Southeast Asian sector during the storm period. Density data obtained by the DMSP F15 satellite at ~800 km altitude and CHAMP satellite at ~380 km altitude were used for interpreting the PB characteristics. Detailed information on the satellites and the instruments on board the satellites can be found in the paper by *Rich and Hairston* [1994] and *McNamara et al.* [2007].

3. Results

3.1. GPS TEC Fluctuations

[9] The coverage of ground-based GPS network available for this study makes it possible to explore the longitudinal and latitudinal difference of PB occurrence. An overview of PB occurrence rates during the storm period is shown in Figure 3. Figure 3 represents the premidnight and postmidnight PB occurrence rates on 7–11 November 2004. The blank areas in the grid maps indicate that in these regions only few GPS TEC data (less than 30 samples of ROTI for each grid) can be obtained to investigate the PB occurrence rate. We remove them from the data set. From Figure 3 it can be clearly seen that PBs were observed on 7 November at premidnight at low latitude (before storm). During the main phases of the storm (8 and 10 November), no PBs were observed on 8 November. When we note the PB occurrence in the second main phase of the storm, the two panels of 10 November (Figure 3) show that high PB occurrence rates occurred at premidnight and postmidnight in Southeast Asia. In the Japanese longitude, the PBs and associated irregularities occurred at a wide latitude range, including equatorial to low and middle latitudes. However, in the close-by longitude Chinese sector, an obvious difference can be seen at latitudes lower than 20°N and the western longitude of 110°E, no PBs were observed. The absence of lower-latitude PBs can also be found from the space-borne satellite observations (see Figure 6). In the Southern Hemisphere Australian sector, the irregularities occurrence rates at premidnight are present as near symmetrical distribution at conjugate latitudes.

[10] Figure 4 illustrates the variation of TEC obtained from the fifteen GPS receivers (marked by solid circles in Figure 3). Figure 4 (left) shows that the rates of TEC (ROT) observed from the GPS receivers (located at the outside

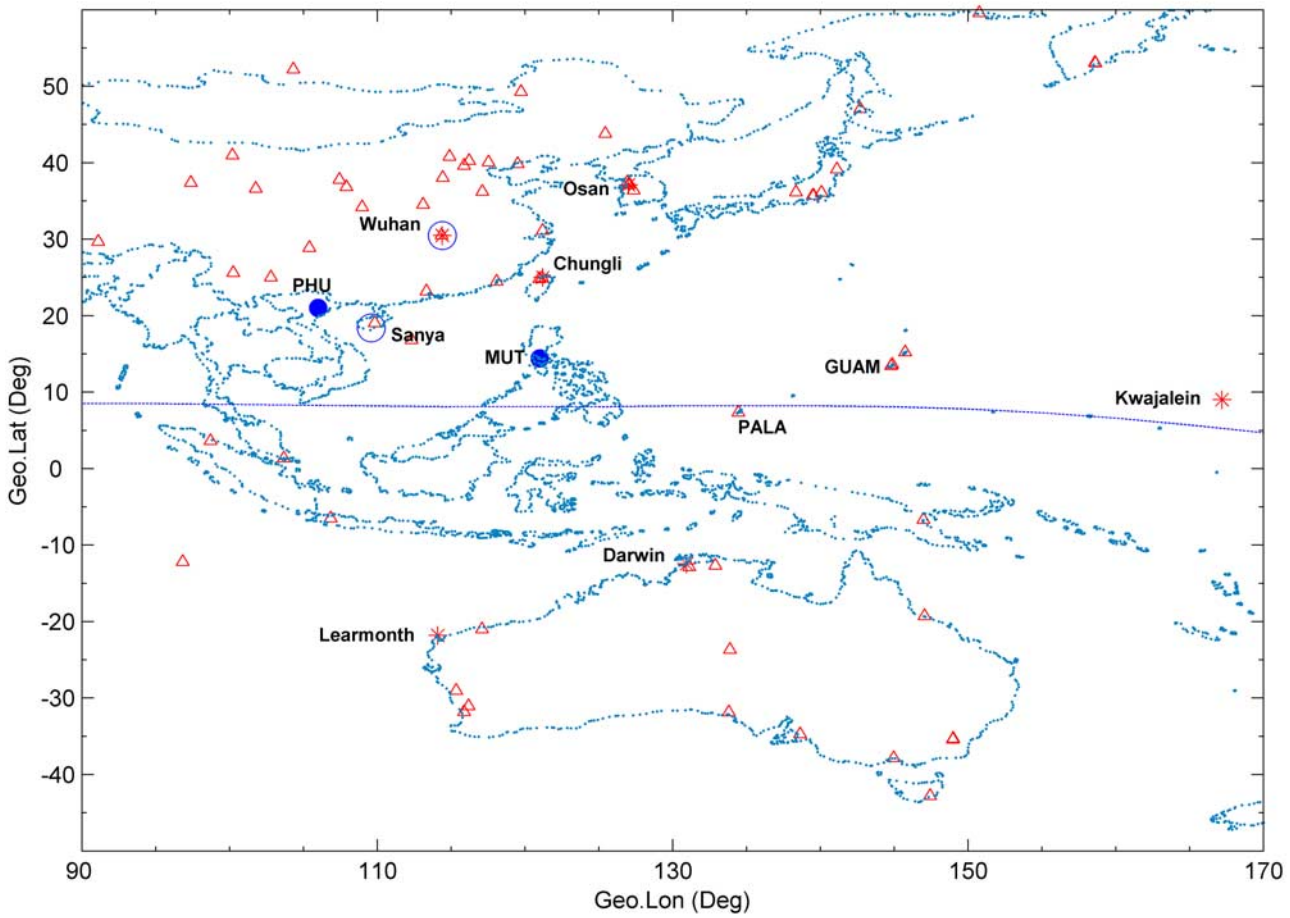

Figure 2. The geographic distribution of the GPS TEC (triangles) and scintillation receivers (open circles), ionosondes (asterisks), and magnetometers (filled circles).

region of high PB occurrence rates) are below 1 TECu/min and reveal that no abrupt TEC fluctuations were detected at these stations. For stations located at the inside region, Figure 4 (middle) shows that increased fluctuations of ROT can be seen. The larger values of ROT reflect the activity of irregularities causing TEC depletions. There is a good consistence between the observations of rapid TEC fluctuation from selected GPS receivers and the PB occurrence rate map of Figure 3. It indicates that in the Northern Hemisphere, the observed irregularities producing TEC depletions were confined in the eastern longitude of 110°E. The meridional observations of 115°E (stations BJFS and WUHN) and 121°E (SHAO and TCMS) show that there is a sequence of irregularities occurrence from higher to lower latitudes. However, in the Southern Hemisphere, near simultaneous rapid TEC fluctuations can be seen from the stations JAB1, ALIC and CEDU in the Australian sector, near the longitude of 133°E. Small TEC fluctuations were found at stations KARR and S021, which located at the edge region of PB occurrence.

[11] A sequence of ROTI maps with one hour interval on 10 November are plotted as a function of geographic longitude and latitude. Figure 5 illustrates the evolution of irregularities during the period 1100–1900 UT. The bold solid lines represent the intersections with the *F* region, at 400-km altitude, of the raypaths from the GPS satellites to the ground stations. The red color represents the ROTI above the threshold of 0.075 TECu/min. The temporal behavior of the ROTI shows that the irregularities seem to be generated in the eastern longitude of 125°E at both

Table 1. Information of Stations From Which Ionogram, Scintillation, and Magnetometer Data Were Collected for This Study

Station Name	Geographic Latitude (deg)	Geographic Longitude (deg)	Magnetic Latitude (deg)	Resolution (min)
Ionogram Data				
Osan	37.1	127.0	27.3	15
Wuhan	30.5	114.4	20.3	15
Chungli	25.0	121.2	14.9	15
Wakkanai	45.4	141.7	36.2	60
Yamagawa	31.2	130.6	21.2	60
Okinawa	26.3	127.8	16.1	60
Kwajalein	9.0	167.2	3.6	5
Darwin	−12.5	131.0	−22.4	15
Learmonth	−21.8	114.1	−32.0	15
Scintillation Data				
Wuhan	30.5	114.4	20.3	1
Sanya	18.4	109.6	7.7	1
Magnetometer Data				
MUT	14.4	121.0	0.64	1
PHU	21.0	106.0	7.1	1

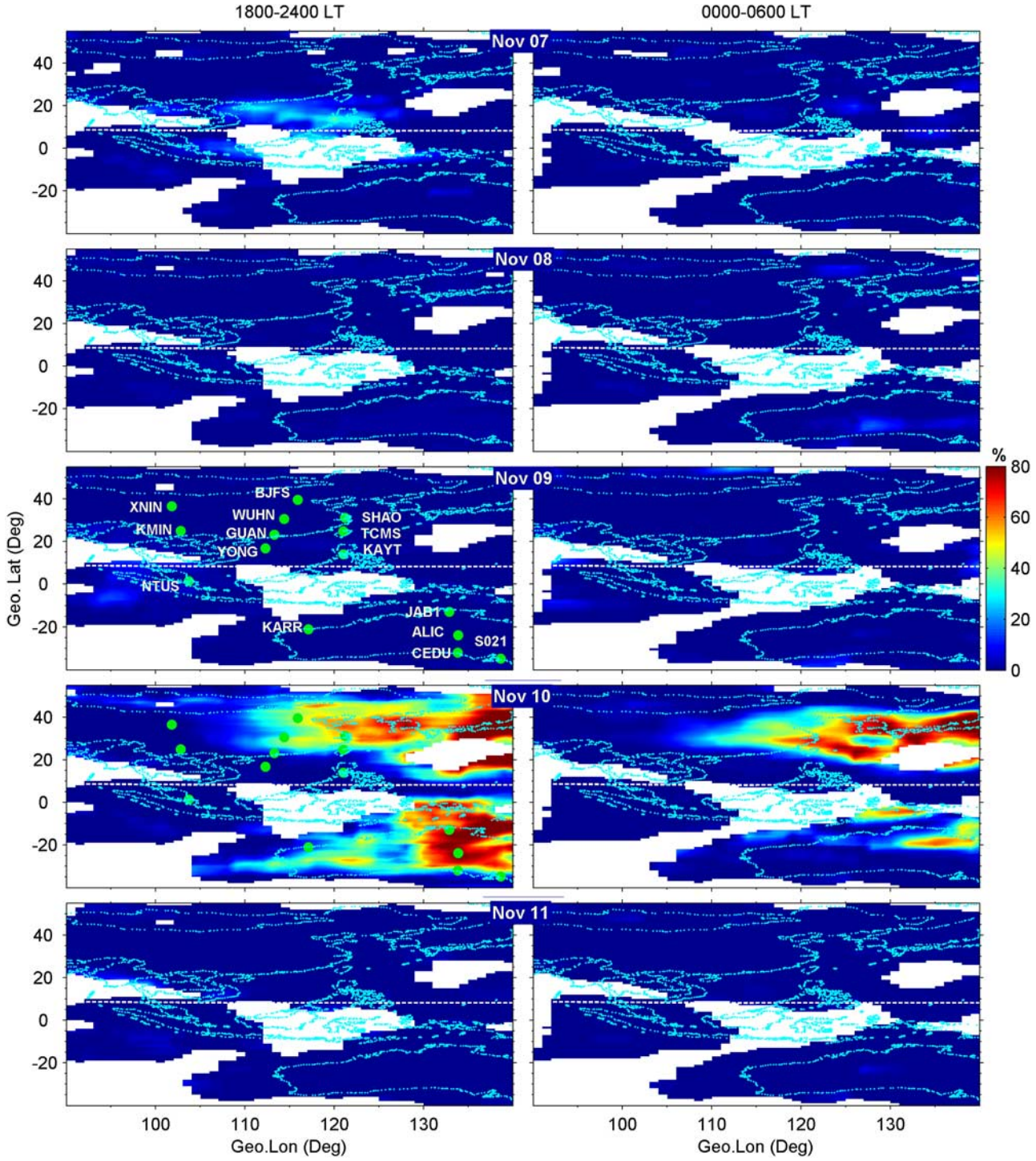

Figure 3. Maps of PB-associated irregularities occurrence rates at premidnight and postmidnight on 7–11 November 2004. The dashed line represents the dip equator.

hemispheres before 1200 UT, over a very large region with east–west dimensions. In the Southern Hemisphere, most middle-latitude irregularities in the western longitude of 125°E were observed before 1500 UT. After that, the irregularities decayed and ceased around 1800 UT. For observations at Northern Hemisphere, the middle-latitude irregularities in the longitudes 115–120°E, 110–115°E and 105–110°E were sequentially observed. A possible westward drift of the irregularities can be seen. Figure 5 (bottom) shows an approximately 5-hour data segment obtained at Wuhan, when measurements were made using three GPS TEC receiving systems spaced in the east–west and south–north directions by separations of about 5 km. The drift velocity can be estimated from the time offset between the three space-aligned receivers, and the detailed process can be found in the paper by *Xu et al.* [2007]. An

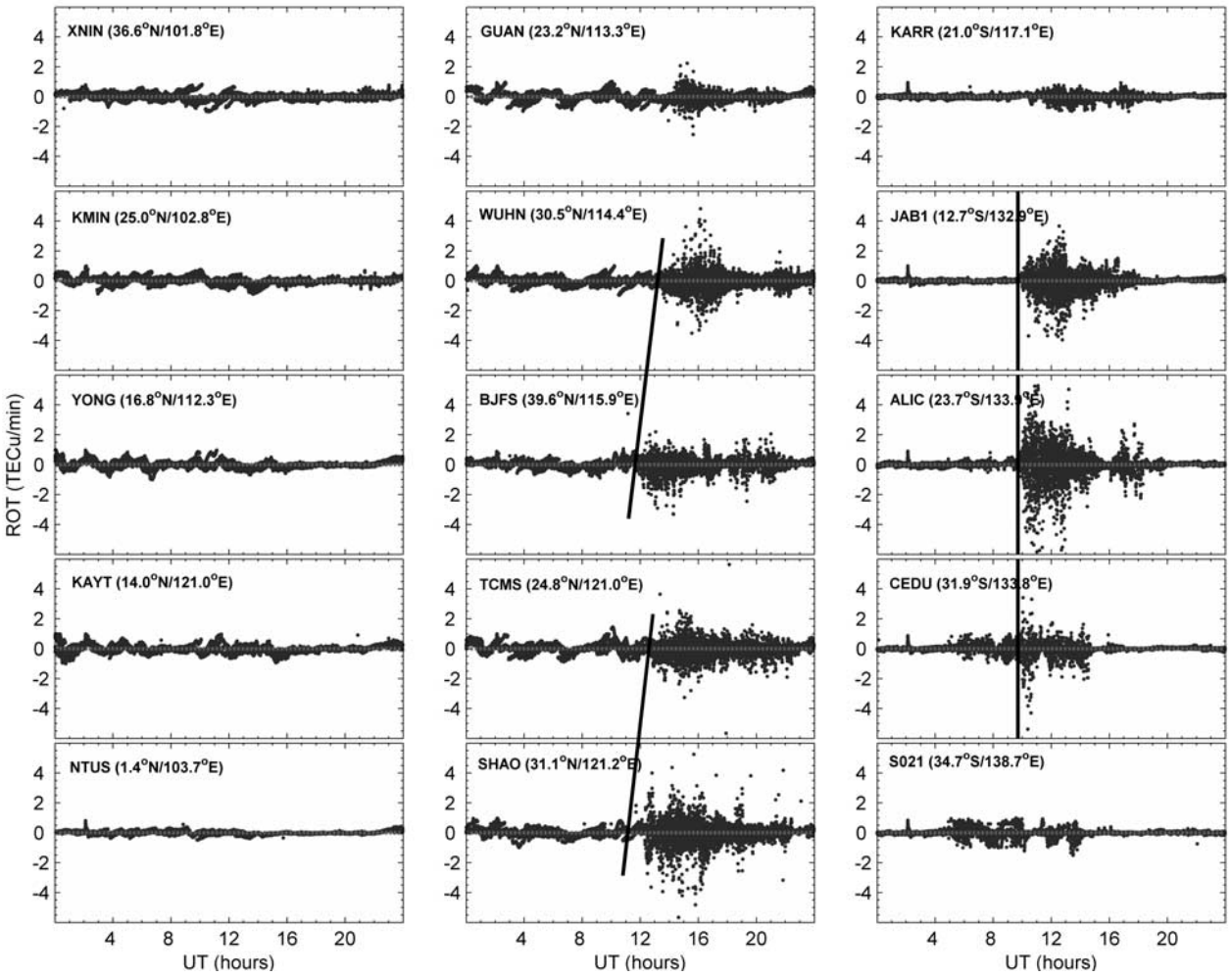

Figure 4. Plots of rate of TEC (ROT) at the fifteen stations for all satellites on 10 November. The geographic locations of selected GPS TEC receivers are shown as green circles in Figure 3.

apparent westward drift between 90 and 35 m/s during the period 1400–1900 UT was shown. These PB-associated irregularities, in an environment of high plasma density, are responsible for generation of intense amplitude scintillations that adversely impact communication and navigation systems, since the steep gradients on the edges of depletions help to generate small-scale irregularities as the bubbles rise to higher altitude (Haerendel, 1974). The following two sections provide the in situ density observations from F15 and CHAMP, and the scintillation measurements from the low- to middle-latitude station Wuhan and low-latitude station Sanya.

3.2. In Situ Density Depletions

[12] Figure 6 shows the satellite passes and measurements of density from DMSP F15 and CHAMP on 7–11 November 2004 in Southeast Asia. The F15 pass moves from the south to the north and the CHAMP pass moves from the north to the south, marked by the arrows in Figure 6 (left). The universal times in the DMSP and CHAMP plots are the times of the beginning and end of the plots. Each plot presents about 30 min and 25 min for DMSP and CHAMP data, respectively. It is noticeable from Figure 6 (top) that during the storm period of 7–11 November, the F15 pass on 7 November observed PBs at low latitude near 122°E longitude. Multiple plasma density depletions within geographic latitude 25°S–45°N and longitude 145°–125°E were detected on 10 November (the second main phase of the storm), marked by the dashed rectangle in the density plots around 1156–1208 UT (see Figure 6, top, 10 November; track d). The CHAMP observations during the second main phase also show large depletions in the two consecutive passes (see Figure 6, middle and bottom, 10 November; track d), respectively, from 1624 to 1649 UT and 1756–1822 UT. The electron density in PBs depleted about 5.5×10^5 cm^{-3}, and was found to exist within the regions of enhanced background electron densities at middle latitude of Northern Hemisphere. In Figure 6 (bottom) we note that PBs were not observed around geographic latitude 0–20°N at 122°E on 10 November, although the succeeding PBs were seen at higher latitude, 20–42°N. The absence of PBs in the lower-latitude regions is consistent with the ground-based TEC measurement. It indicates that for the latitude region lower than 20°N, no PBs and associated irregularities can be seen from ground-based and space-borne

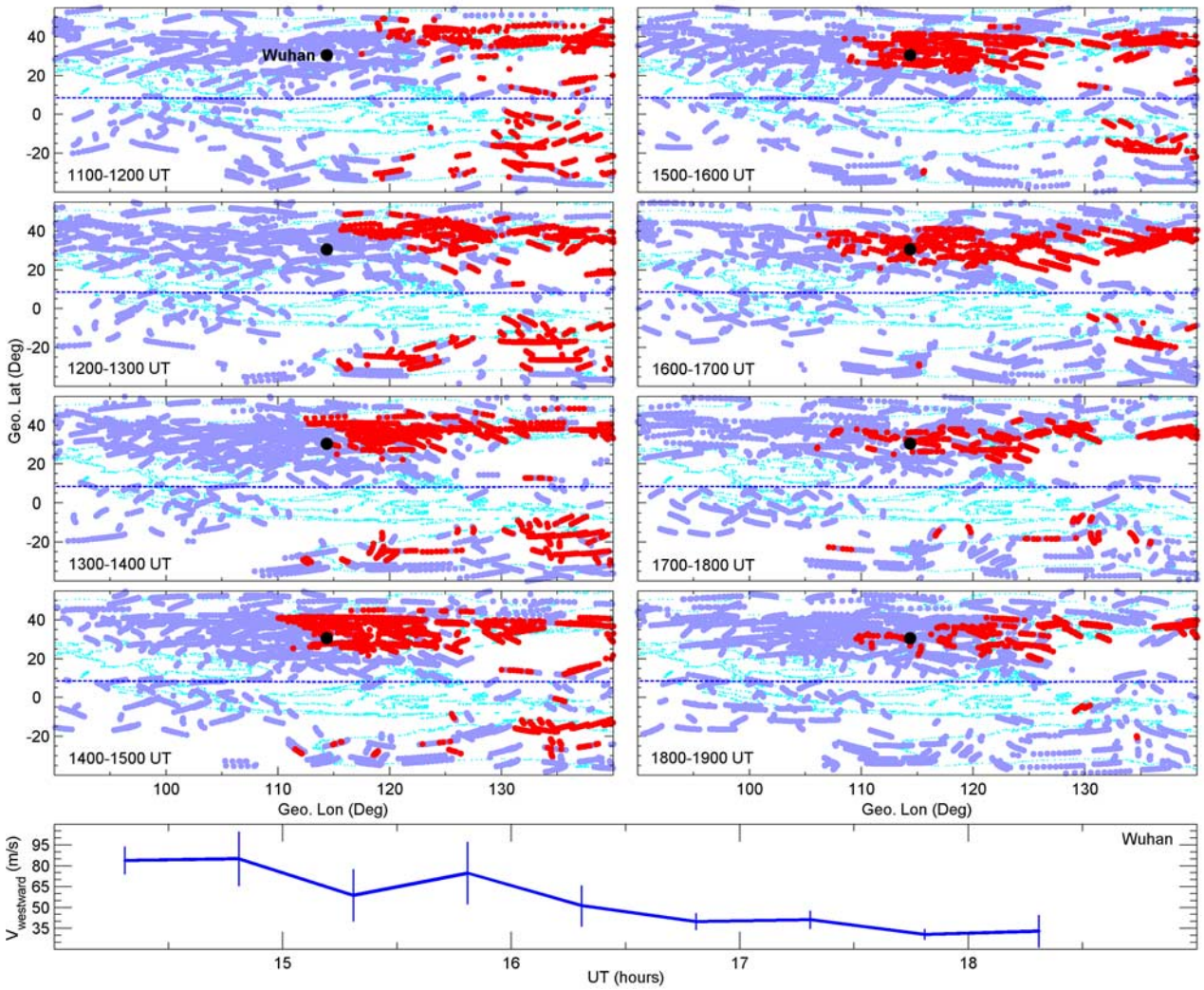

Figure 5. (top) ROTI maps showing the temporal and spatial evolution of PB-associated irregularities during the period 1100–1900 UT. Red markers represent the ROTI above the threshold 0.075 TECu/min. (bottom) Westward drift velocity obtained at Wuhan by space-aligned GPS TEC receivers on 10 November.

measurements in the Chinese longitude, about western longitude of 125°E.

3.3. GPS Amplitude Scintillations

[13] The continuous scintillation measurements made at Wuhan and Sanya are useful for tracking the onset of scintillation at middle and low latitudes. Figure 7 illustrates the variation of the amplitude scintillation index S_4 at L-band recorded at both stations from GPS satellites. The scintillations above the threshold of 0.2 were marked by the red dots. The S_4 index, obtained from the ratio of the standard deviation of signal intensity fluctuation normalized to the average signal intensity, quantifies the strength of amplitude scintillation and typically lies in the range 0 to 1. Figure 7 (top left) presents that an impulsive onset of amplitude scintillation occurred at 1300 UT with a maximum value 1 near 1600 UT (~2400 LT), possibly shows saturated scintillation in the midnight at Wuhan station. According to scintillation theory [*Yeh and Liu*, 1982], S_4 depends on the electron density deviation of the ionospheric irregularities and also on the thickness and height of the irregularity layer. When the density depletions develop, the irregularity layer reaches the *F* region peak where the plasma density is much higher, giving rise to larger density deviations and inducing stronger scintillations. At L band frequency range, amplitude scintillations are caused by tens to hundreds of meters scale-size irregularities. Combining the TEC fluctuations considered at previous section, we expect that the small-scale irregularities producing scintillation coexist with the large-scale PB structures in the middle-latitude ionosphere. Close to station Wuhan, the CHAMP orbit (track d in Figure 6) recorded a series of PBs. The comparison of observations presented by in situ satellites and ground-based scintillation receivers shows that the ionospheric irregularities rise up to the topside ionosphere and produce a series of plasma density depletions in the middle-latitude regions. Figure 7 (bottom left) shows

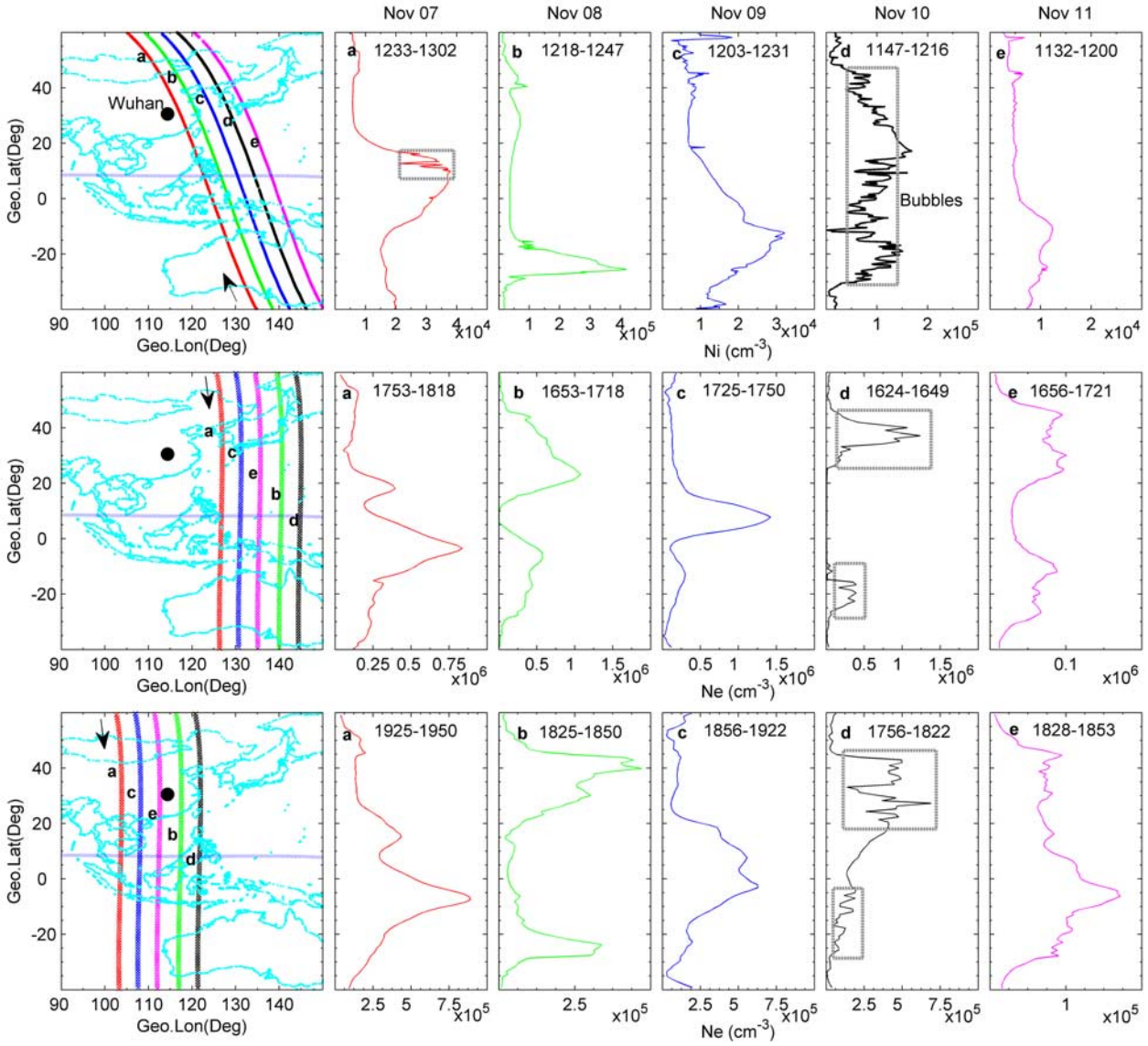

Figure 6. In situ density measurements from DMSP F15 and CHAMP. (left) Ground tracks a–e of F15 and CHAMP crossing the area during the period 7–11 November. The thin dashed line represents dip equator. (right) Density measurements along the satellite tracks.

that station Sanya did not observe any scintillation during the storm day at the 400-km intersection point range of 10–22°N, 102–118°E.

3.4. Ionosonde Spread *F*

[14] To fully understand the processes that control the onset of PB-associated irregularities, it is helpful to investigate time development and spatial distribution of this *F* region phenomenon. Ionosondes collecting ionogram with a time interval of 15 min at four stations, Osan, Wuhan, Chungli and Darwin during the storm period were analyzed. We categorized the spreading echo traces into four types, RSF (range spread *F*) I, II and FSF (frequency spread *F*) I, II to illustrate the generation and evolution of spread *F* irregularities [*Lee et al.*, 2005a, 2005b; *Chen et al.*, 2006]. A sequence of RSF-I, RSF-II and FSF-I, FSF-II demonstrates the *F* region irregularities initially develop at the lower part of the *F* region (RSF-I). After spread *F* initiation, the irregularities ascend to higher altitudes and then distribute in whole *F* region (RSF-II). While the irregularities at lower altitudes dissipate, they still can persist at higher altitudes (FSF-I, FSF-II). The spread *F* intensity is estimated from the thickness of spread layer in the ionogram traces as *Rodrigues et al.* [2004] reported. The weak, moderate and strong spread echoes are associated with the thickness <100 km, 100–200 km and >200 km, respectively.

[15] Figure 8 shows foF2 and hmF2 variations, and examples of ionograms on 10 November for stations Osan, Wuhan and Chungli. The diurnal variations on geomagnetic quiet day 6 November are denoted as thin lines for comparison. It is clearly seen from Figure 8 (left) that the foF2 variations at Osan start an increase at 1000 UT on 10 November. The spread *F* irregularities initiated at the declining phase of hmF2. As shown in the ionograms, we

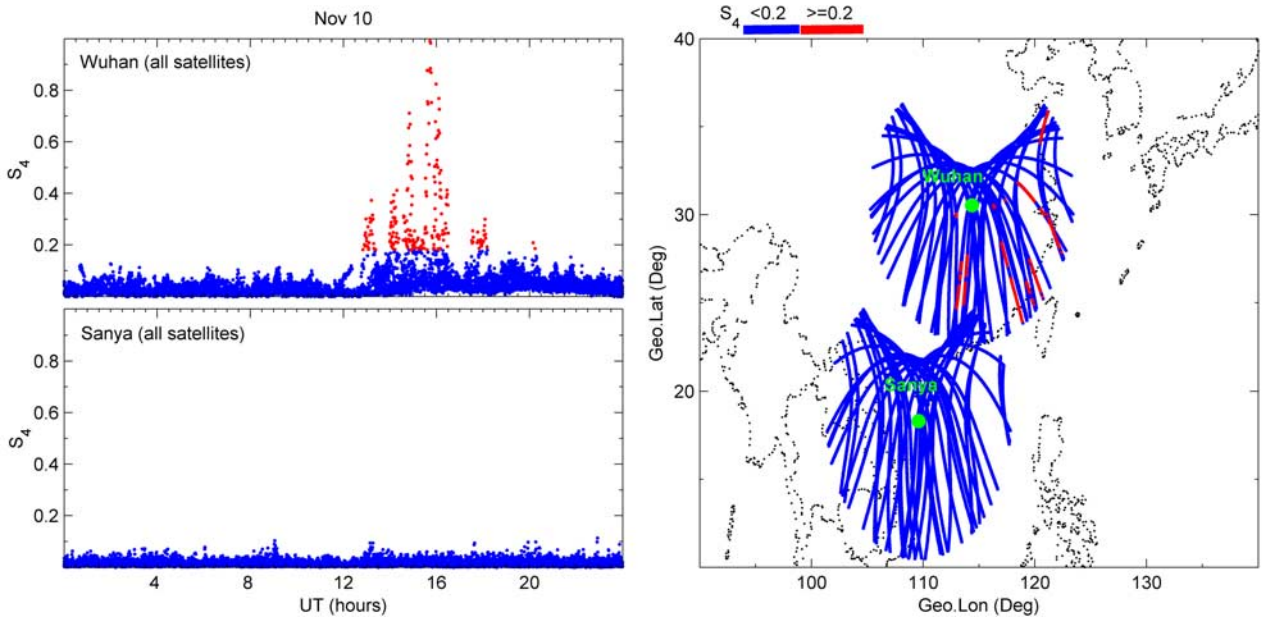

Figure 7. (left) GPS amplitude scintillations (S_4 index) for all satellites obtained at Wuhan and Sanya on 10 November. (right) A map of GPS satellite tracks assuming a thin shell ionosphere at 400 km altitude. Red markers represent the S_4 index above 0.2.

note that strong RSF-I at Osan was first observed in the lower part of bottom-side *F* region at 1115 UT. The spread layer located at about 350–600 km altitude. Subsequently, the spread layer thickness decreased and moderate RSF-I was presented at 1200 UT. Then the spread *F* irregularities evolved as RSF and FSF, and continued to exist until the morning hours, about 2330 UT (0730 LT). The period of spread *F* irregularities is present as the horizontal bar in Figure 8 (top). At Darwin, a middle-latitude station of Southern Hemisphere, strong RSF-I were also found initiating in the lower part of bottom-side *F* region around 1115 UT. As shown in Figure 9, this initial time of bottom-side spread *F* irregularities is similar to Osan observation. This implies that the spread *F* irregularities at the two stations were locally generated.

[16] After about three hours from the onset of Osan spread *F* irregularities, spread *F* at Wuhan were found to initiate at 1400 UT. Figure 8 (middle) shows the evolution of Wuhan spread *F* on 10 November. The foF2 and hmF2 variations are also shown in Figure 8. Wavelike oscillations in foF2 and hmF2 can be seen, which were possible results of traveling atmospheric disturbances [*Lee et al.*, 2004]. In addition, the wave structures were observed by DE-2 satellite at altitudes about 300 km, and suggested to be driven by gravity waves in the neutral atmosphere [*Earle et al.*, 2008]. A disagreement can be seen from the evolution of spread *F* at the two stations Wuhan and Osan. As shown in the ionograms of Figure 8 (middle), RSF-II was first observed and the distribution of spread *F* echoes filled with all bottom side of *F* region around 1400–1415 UT at Wuhan. During the period 1430–1500 UT, strong spread echoes were found in the lower part of bottom-side *F* region. We believe that at this moment the freshly generated spread *F* irregularities formed at the bottom-side *F* region. This probably indicates a simultaneous observation of old and freshly generated spread *F* irregularities. Combined the drift measurements by space-aligned GPS receivers at Wuhan, the first observed RSF-II were possible irregularities transported from the eastern longitude of Wuhan owing to the westward drift velocity. The spread *F* irregularities ceased after sunrise at Wuhan, about 0030 UT (0830 LT) on 11 November.

[17] Figure 8 (right), shows the measurements from Chungli ionosonde, which detected FSF at 1415–2315 UT. During this period, no obvious difference can be seen from the quiet (6 November) and storm time (10 November) hmF2 variations. The ionograms of Figure 8 (right) show that the spread *F* irregularities existed near the *F* layer peak, and no bottom-side irregularities were observed. FSF were also observed from Learmonth ionosonde station in the Australian sector during the period 1315–2145 UT (the figure is not shown here). From comparison of observations in New Zealand with those obtained in Australia, *King* [1970] concluded that frequency spreading is simply the decay product of the range spreading. Here the absence of RSF and presence of FSF in the two stations Chungli and Learmonth imply that the FSF are possible old irregularities which were diffused from the close-by region.

4. Discussion

[18] Multiple instrument observations on 10 November illustrate the occurrence of PB-associated irregularities over a wide longitude range at latitudes higher than 20°N, including most part of China and Japan (the eastern longitude of 110°E). However, at equatorial latitude, PBs were observed at a relatively narrow longitude range, confined in the eastern longitude of 125°E. Possible reasons inducing this difference in longitude and latitude are discussed in the following.

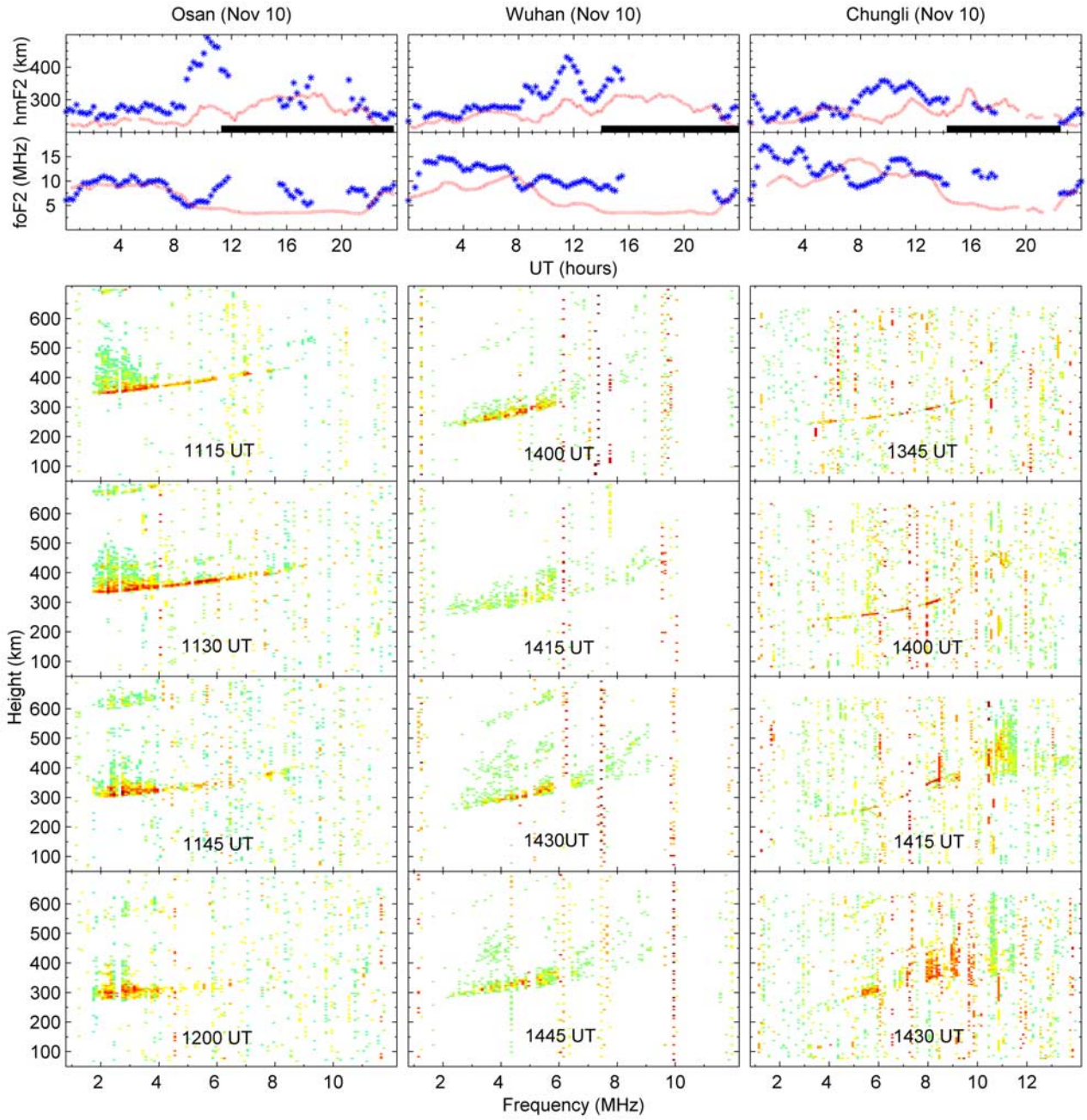

Figure 8. Examples of ionograms obtained at Osan, Wuhan, and Chungli on the night of 10 November 2004. Variation of hmF2 and foF2 is shown at top. The periods of spread *F* (RSF and FSF) are shown by horizontal bars. The diurnal variations on geomagnetic quiet day 6 November are denoted as thin lines for comparison.

4.1. Prompt Penetration Electric Field Effects

[19] During storms, the low-latitude ionospheric electric fields can be promptly disturbed by penetration electric fields. Past studies have shown that average empirical equatorial prompt penetration electric fields are in good agreement with the predictions from global convection models [*Fejer and Scherliess*, 1997; *Fejer and Emmert*, 2003]. On the other hand, the large variability of these electric fields with different magnitudes and lifetimes is not well understood [*Huang et al.*, 2005, *Wei et al.*, 2008]. A complex relationship between prompt penetration and solar wind electric fields and polar cap potentials during the November 2004 geomagnetic storm were reported by *Fejer et al.* [2007].

[20] In the equatorial and low-latitude region, one of the necessary conditions for the generation of *F* region irregularities is that the *F* layer should be lifted to a higher altitude, where the R-T mode becomes unstable and then forms PB-associated irregularities. The *F* layer height is largely determined by the equatorial vertical drift velocity, which is driven by the zonal electric field via the E $\times$ B drift

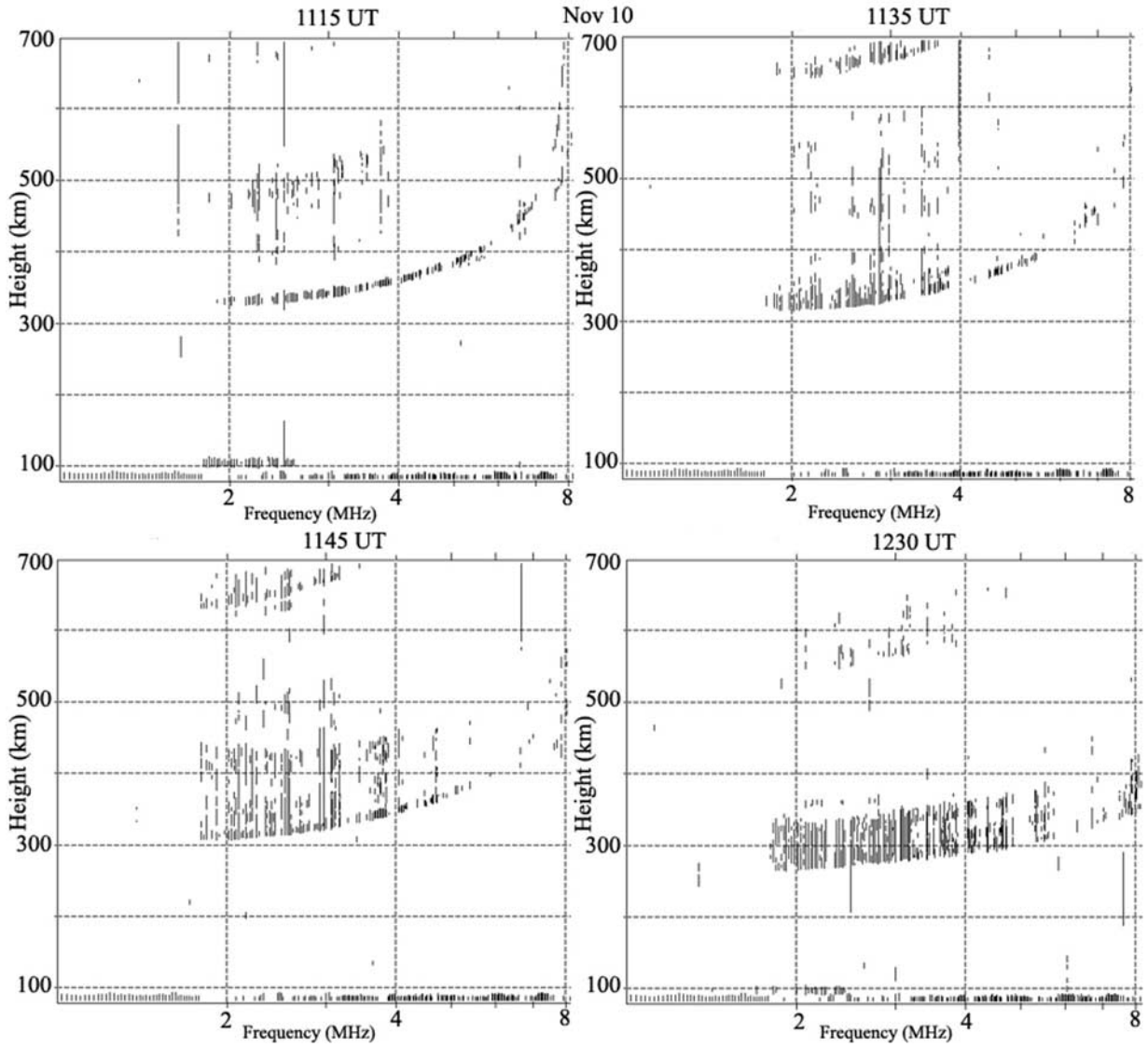

Figure 9. Examples of ionograms obtained at Darwin on the night of 10 November 2004.

[*Dabas et al.*, 2003]. Several studies have shown that the variation of vertical E × B drift velocity can be estimated from the simultaneous measurements of the horizontal component (H) of the Earth's magnetic field at equatorial and off equatorial stations in nearly the same longitude sector [*Anderson et al.*, 2002], from in situ satellites [*Oyekola*, 2006], and from ionosonde observations of h'F (the virtual height of the *F* layer) and hmF2 [e.g., *Bittencourt and Abdu*, 1981; *Liu et al.*, 2003; *Oyekola and Oluwafemi*, 2008; *Oyekola et al.*, 2008]. Here we complement the ground-based magnetic field observations ΔH ($H_{mut} - H_{phu}$) from MUT and PHU, and the ionosonde measurements from Kwajalein to investigate the effects of prompt penetration electric fields on PB-associated irregularities occurrence.

[21] As shown in Figure 10, the first, second, and third panels illustrate the variations of hmF2, h'F and ΔH on 7–11 November. A detailed survey of ΔH variations during the storm period has been performed by *Fejer et al.* [2007]. Now we confined our attention to the second main phase of storm (10 November), when strong PB-associated irregularities were detected. On 10 November, the first and second panels of Figure 10 show a rapid increase of hmF2 and h'F about 350 km, associated with a large upward drift velocity about 83 m/s with an average during the period 0630–0740 UT. In the evening sector, when the upward drifts are larger than 5–10 m/s and 15–20 m/s near the solar minimum, weak and strong irregularities may be generated in the *F* region, respectively [*Fejer et al.*, 1999]. After the abrupt increase of h'F and hmF2, the ionograms at Kwajalein show strong spread echoes which initiated at 0730 UT (1830 LT), and continued for 12 h. The period of spread *F* irregularities is marked as the horizontal bar in Figure 10 (first panel). It is clearly seen from the second panel of Figure 10 that the magnetic field data ΔH also show very large positive perturbations around 0700 UT. The simultaneous abrupt increases of ΔH and h'F imply strengthen of eastward electric field. This behavior is most likely associated with the effect owing to the prompt penetration of an eastward electric field into the equatorial ionosphere [*Li et al.*, 2008]. The fourth and fifth panels of

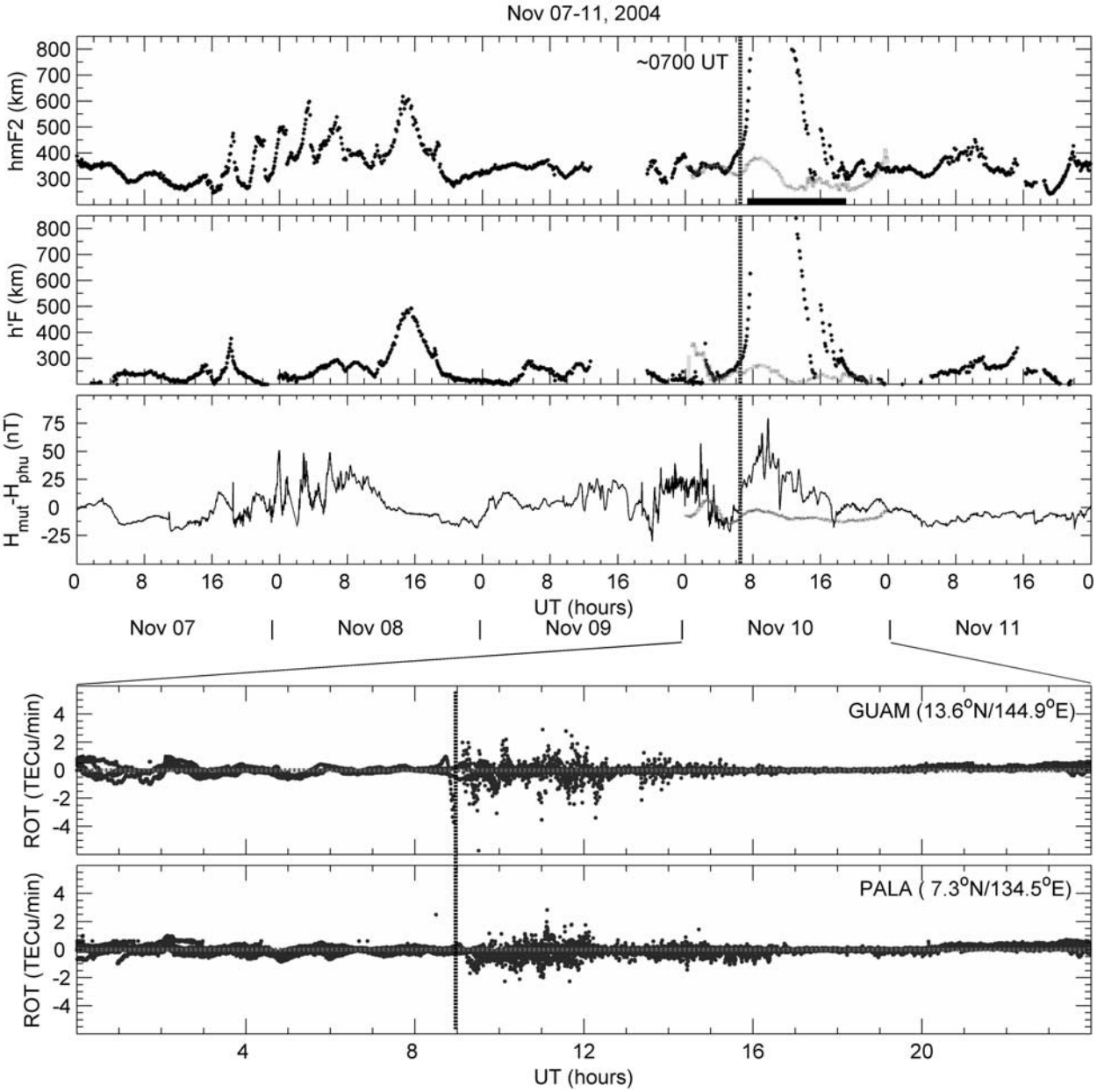

Figure 10. The variations of hmF2 and h'F observed at Kwajalein, ΔH parameter (MUT-PHU), during the period 7–11 November 2004. The diurnal variations on geomagnetic quiet day 6 November are denoted as thin lines for comparison. The periods of spread *F* (RSF and FSF) are shown by a horizontal bar. The fourth and fifth panels show the variation of ROT obtained at GUAM and PALA on 10 November.

Figure 10 show the variations of TEC fluctuation parameters ROT obtained from stations GUAM and PALA. The two sites are located at equatorial and low latitude in the Japanese longitude (see Figure 2). The ROT variations show that the PBs and associated irregularities initiated at about 0900 UT (∼1800 LT). These observations indicate that involved mechanism is the prompt penetration of an eastward electric field that produces upward disturbance vertical drifts during the postsunset period. This extra push, favors the conditions for the generation of equatorial irregularities through destabilizing the R-T instability. For the western longitude of 125°E, the sunset terminator transited these regions after 1000 UT. Thereafter the prompt penetration probably decayed and the strength of eastward electric field was not enough to elevate the *F* layer to higher altitude in these regions. The difference in irregularities occurrence between the two close-by longitudinal sectors suggests that the effects of prompt penetrating electric fields of magnetospheric origin are localized in longitude [*Li et al.*, 2008; *Tulasi Ram et al.*, 2008] and do produce substantial differences in irregularity activity at regions separated by few hundred kilometers [*Basu et al.*, 2001].

[22] When we note the onset time of higher-latitude (above 20°N) PB-associated irregularities in the Chinese longitude sector, the irregularities were observed at a latitude sequence from higher to lower latitude. The onset

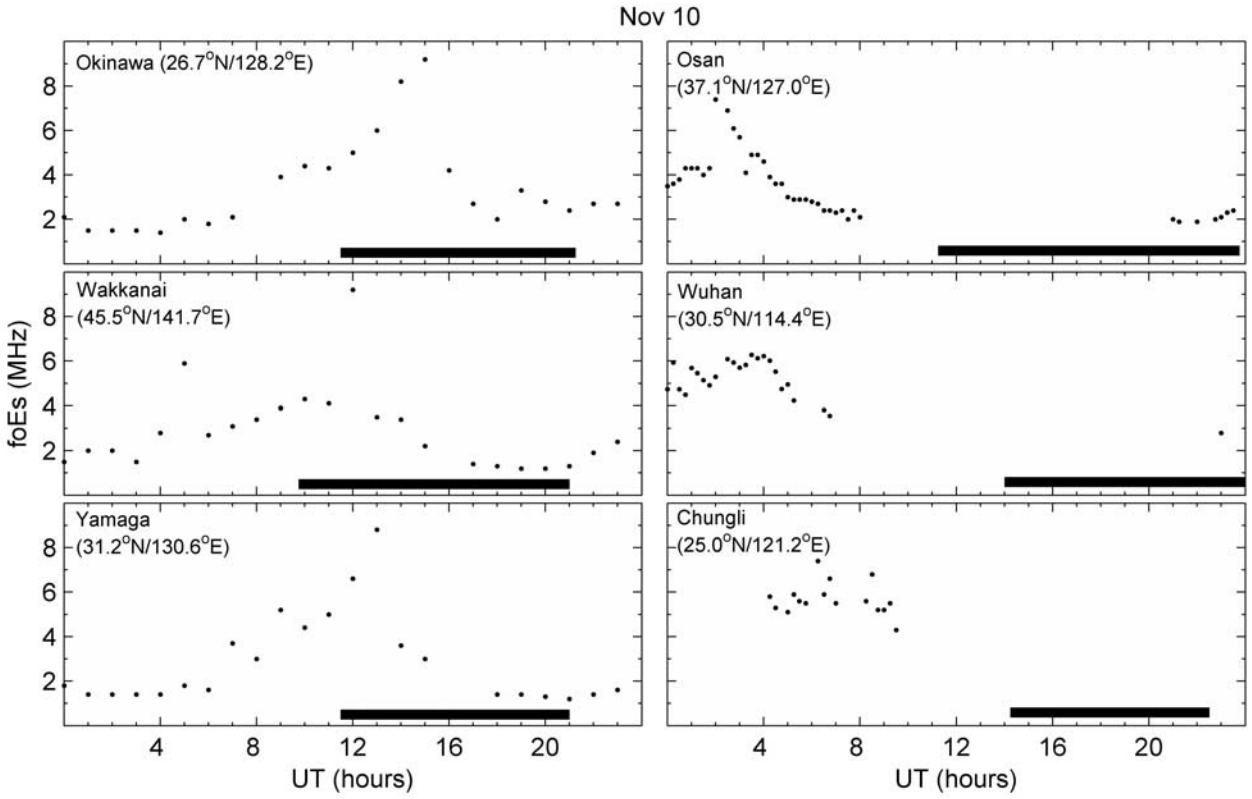

Figure 11. The variations of foEs obtained from the east Asian ionosondes on 10 November. The periods of spread *F* (RSF and FSF) are shown by horizontal bars.

time is about 1115 UT at Osan and 1400 UT at Wuhan (see Figure 8). The sequential order of irregularities occurrence is similar to that reported by *Sahai et al.* [2009b]. They presented the onset time of irregularities in the Japanese sector at Wakkanai (45.5°N, 141.7°E) about 0945 UT and at Kokubunji (35.7°N, 139.5°E) and Okinawa (26.2°N, 127.8°E) about 1130 UT. During three intense magnetic storms, *Basu et al.* [2005] investigated the evolution of plasma density structures at middle and low latitudes, and found that the onset of low-latitude scintillation is delayed from that at middle latitudes by about 20 min. This time delay should be caused by the instantaneous electric field penetration and plasma instability growth time of equatorial irregularities. However, the irregularities observed at middle and low latitude in the Chinese sector on 10 November in our case does not belong to the above situations, since the irregularities triggered by the prompt penetration of magnetospheric and high-latitude electric fields to middle and low latitudes, or the irregularities extended from equatorial to low latitude along the magnetic field lines do not need several hours. Specially, no equatorial PB-associated irregularities were observed in the Chinese longitude.

4.2. Sporadic *E* and TIDs

[23] Middle-latitude spread *F* irregularity observations have been widely explained as the Perkins instability, which is the instability of the *F* layer to an altitude modulation horizontally distributed as a plane wave [*Perkins*, 1973] and has been simulated by *Yokoyama et al.* [2008] with a three-dimensional numerical model. The azimuthal orientation of the plane wave phase fronts that maximizes the growth rate depends on the background electric field direction. Perkins showed that the northeast electric field direction in the middle-latitude evening is suitable for the instability to occur. The vertical gradient in neutral density coupled with a northward component of the electric field (or equivalent neutral wind) contributes the free energy for the instability through a Pedersen current-driven polarized process. Yet the linear growth rate of that instability appears too weak to account for the observations. Recently *Tsunoda and Cosgrove* [2001] pointed out that *F* layer and sporadic *E* (*Es*) layer in the nighttime middle-latitude ionosphere should be considered electrodynamically as a coupled system in light of the presence of a Hall polarization process in *Es* layers. With the discovery of an instability of *Es* layers that has growing modes with skewed azimuthal alignments similar to those of the Perkins instability [*Cosgrove and Tsunoda*, 2003], several investigators have considered the behavior of these two instabilities as a coupled system [e.g., *Haldoupis et al.*, 2003; *Kelley et al.*, 2003]. In this study, the *Es* layer observations from ionosondes on 10 November are shown in Figure 11. It illustrates the appearance of *Es* layer at Okinawa, Wakkanai and Yamaga, and the absence at Osan, Wuhan and Chungli, respectively. During the period of spread *F* irregularities (marked by the bold solid lines), the layer in the *E* region and hence the conductivity encountered an increase at night for the three ionosode stations in the Japanese sector. It shows there is a possible link between simultaneous occurrences of middle-latitude spread *F* and sporadic *E*. A physical interpretation of the

E-F coupled-layer instability has been investigated by *Cosgrove et al.* [2004]. The maximum growth rates for the *Es* layer and Perkins instability are found to exist at the same phase front orientation which is aligned northwest to southeast in the Northern Hemisphere. Moreover, a close link of mesoscale middle-latitude spread *F* with patchy *Es* layers owing to gravity wave induced large-scale electric fields mapping the *E* region to the *F* region is shown [*Haldoupis et al.*, 2003]. Here the simultaneous observations of spread *F* and sporadic *E* at the three stations possibly indicate that under suitable conditions the coupling between the Perkins and *Es* layer instabilities enhanced the growth rate for middle-latitude ionospheric irregularities.

[24] Also, the Perkins instability can be significantly enhanced owing to gravity waves seeding of middle-latitude ionosphere [*Kelley and Fukao*, 1991; *Huang et al.*, 1994; *Saito et al.*, 1998]. Gravity waves can produce two kinds of ionospheric irregularities. The passive ionospheric responses to gravity waves are the TIDs [*Yeh and Liu*, 1974]. Another is the plasma instabilities initiated by gravity waves, which act as an external driving force and seed active plasma dynamics and instability growth. *Huang et al.* [1994] and *Miller* [1997] suggested that seeding by atmospheric gravity waves is an important factor in the generation of middle-latitude spread *F* irregularities. In the east Asian sector, *Pirog et al.* [2007] reported large-scale ionospheric disturbances of 8 and 10 November 2004, determined according to the data of both ground-based GPS network and the GPS receiver onboard the CHAMP satellite. The TIDs propagate with a southwest velocity of about 400 m/s on 10 November. Also, the TEC map from a dense GPS network in Japan on this day shows the presence of TIDs, which are suggested to be related to the atmospheric gravity waves launched by enhanced Joule heating in the auroral zone [*Sahai et al.*, 2009b]. When we note the spread *F* occurrence sequence presented in this study, it shows consistent results with observations reported by *Bowman* [1981] that nearly all observations of middle-latitude spread *F* ionogram traces for which a direction of propagation have been measured were seen to propagate equatorward and westward. These together possibly suggest that the TIDs are responsible for the initiation of spread *F* irregularities observed in the Chinese longitude on 10 November. In the Japanese longitude, the observed irregularities at middle latitude may also be manifestations of gravity wave-Perkins instability resonance [*Huang et al.*, 1994] and coupling of *Es* layer and Perkins instabilities.

5. Summary

[25] In this paper, we have analyzed and presented the characteristics of PB occurrence in Southeast Asia on the basis of the observations of ground-based and space-bone satellites during the super storm of 7–11 November 2004. The main results are as follows:

[26] 1. Intense PBs and associated irregularities producing scintillation are found at premidnight and postmidnight in Southeast Asia during the second main phase of the storm (10 November). The irregularities occurred at a wide latitude range, including equatorial to low and middle latitudes in the Japanese longitudes. However, in the close-by longitude Chinese sector, an obvious difference can be seen at the latitude lower than 20°N and the western longitude of 110°E, no PBs were observed. In the Southern Hemisphere Australian sector, the irregularity occurrence presents a near symmetrical distribution in conjugate latitudes at premidnight.

[27] 2. Observations of GPS TEC fluctuations and ionosonde ionograms show the PB-associated irregularities drift with a westward velocity and present an equatorward occurrence sequence in the Northern Hemisphere. However, the near simultaneous rapid TEC fluctuations observed from several GPS stations in the Australian sector imply that such an occurrence sequence from higher to lower latitude is not apparent in the Southern Hemisphere.

[28] 3. Combined analysis of the data from the GPS TEC receivers, magnetometers and ionosonde show that the prompt penetration of magnetospheric electric field to equatorial ionosphere favors the R-T instability growth rate after sunset, and trigger the development of equatorial and low-latitude PBs on 10 November in the Japanese and eastern longitudes. But the irregularities observed at middle and low latitude in the close-by longitude Chinese sector is not induced by the prompt penetration since there is an onset time delay of several hours and the absence of equatorial PBs in the sector.

[29] 4. Comparing the irregularities occurrence sequence and the direction of TIDs propagation in the Northern Hemisphere on 10 November, it is found that the observation shows consistent result with the equatorward and westward occurrence sequence of spread *F* reported by *Bowman* [1981]. Moreover, a close link of middle-latitude spread *F* with strong sporadic *E* layers can be seen in the Japanese sector, where the sporadic *E* layer encountered an increase during the period of Spread *F* irregularities occurrence. These possibly suggest that the observed irregularities at middle latitude may be manifestations of gravity wave-Perkins instability resonance and coupling of *Es* layer and Perkins instabilities.

[30] 5. The absence and presence of PBs at equatorial and low latitudes in the Chinese longitude provide evidence that the storm-time low-latitude PB-associated irregularities cannot be simply explained as the extension of equatorial PBs along the magnetic field lines or the triggering effects of storm-time PPEFs. It may also come from the diffused irregularities which were resulted from the Perkins instability at close-by region.

[31] **Acknowledgments.** This research is supported by the Natural Science Foundation of China (40774091, 40574072, 40725014), National Important Basic Research Project (2006CB806306), and the Open Research Program of State Key Laboratory of Space Weather, CAS. The authors acknowledge IGS and University of Texas at Dallas for providing the GPS TEC and F15 density data, respectively. Ionospheric data are provided from NIICT, DIDB, and IPS. IMF data are obtained from CDAWEB. We thank D. Cooke and C. Roth for processing the CHAMP PLP data. The CHAMP mission is supported by the German Aerospace Center in operation and by the Federal Ministry of Education and Research in data processing. J. S. Xu is supported by the Natural Science Foundation of China (40874085).

[32] Zuyin Pu thanks the reviewers for their assistance in evaluating this paper.

References

Aarons, J. (1993), The longitudinal morphology of equatorial F-layer irregularities relevant to their occurrence, *Space Sci. Rev.*, *63*, 209–243, doi:10.1007/BF00750769.

Abdu, M. A. (1997), Major phenomena of the equatorial ionosphere–thermosphere system under disturbed conditions, *J. Atmos. Sol. Terr. Phys.*, *59*, 1505–1519, doi:10.1016/S1364-6826(96)00152-6.

Abdu, M. A., I. S. Batista, H. Takahashi, J. MacDougall, J. H. Sobral, A. F. Medeiros, and N. B. Trivedi (2003), Magnetospheric disturbance induced equatorial plasma bubble development and dynamics: A case study in Brazilian sector, *J. Geophys. Res.*, *108*(A12), 1449, doi:10.1029/2002JA009721.

Afraimovich, E. L., et al. (2006), Large-scale disturbances of auroral origin during strong magnetic storms of October 29–31, 2003 and November 7–11, 2004, according to the data of the GPS network and ionosondes, *Geomagn. Aeron.*, *46*(5), 603–608, doi:10.1134/S0016793206050070.

Anderson, D., A. Anghel, K. Yumoto, M. Ishitsuka, and E. Kudeki (2002), Estimating daytime vertical E × B drift velocities in the equatorial *F* region using ground-based magnetometer observations, *Geophys. Res. Lett.*, *29*(12), 1596, doi:10.1029/2001GL014562.

Balan, N., H. Alleyne, S. Walker, H. Reme, I. McCrea, and A. Aylward (2008), Magnetosphere–ionosphere coupling during the CME events of 07–12 November 2004, *J. Atmos. Sol. Terr. Phys.*, *70*, 2101–2111, doi:10.1016/j.jastp.2008.03.015.

Basu, S., S. Basu, E. MacKenzie, and H. E. Whitney (1985), Morphology of phase and intensity scintillations in the auroral oval and polar cap, *Radio Sci.*, *20*, 347–356, doi:10.1029/RS020i003p00347.

Basu, S., et al. (2001), Ionospheric effects of major magnetic storms during the International Space Weather Period of September and October 1999: GPS observations, VHF/UHF scintillations, and in situ density structures at middle and equatorial latitudes, *J. Geophys. Res.*, *106*, 30,389–30,413, doi:10.1029/2001JA001116.

Basu, S., S. Basu, K. M. Groves, E. MacKenzie, M. J. Keskinen, and F. J. Rich (2005), Near-simultaneous plasma structuring in the midlatitude and equatorial ionosphere during magnetic superstorms, *Geophys. Res. Lett.*, *32*, L12S05, doi:10.1029/2004GL021678.

Bhattacharyya, A., S. Basu, K. M. Groves, C. E. Valladares, and R. Sheehan (2001), Dynamics of equatorial *F* region irregularities from spaced receiver scintillation observations, *Geophys. Res. Lett.*, *28*, 119–122, doi:10.1029/2000GL012288.

Bittencourt, J. A., and M. A. Abdu (1981), A theoretical comparison between apparent and real vertical ionization drift velocities in the equatorial F region, *J. Geophys. Res.*, *86*, 2451–2454, doi:10.1029/JA086iA04p02451.

Bowman, G. G. (1981), The nature of ionospheric spread F irregularities in middle latitude regions, *J. Atmos. Terr. Phys.*, *43*, 65–70, doi:10.1016/0021-9169(81)90010-6.

Burke, W. J., L. C. Gentile, C. Y. Huang, C. E. Valladares, and S. Y. Su (2004), Longitudinal variability of equatorial plasma bubbles observed by DMSP and ROCSAT-1, *J. Geophys. Res.*, *109*, A12301, doi:10.1029/2004JA010583.

Chen, W. S., C. C. Lee, J. Y. Liu, F. D. Chu, and B. W. Reinisch (2006), Digisonde spread *F* and GPS phase fluctuations in the equatorial ionosphere during solar maximum, *J. Geophys. Res.*, *111*, A12305, doi:10.1029/2006JA011688.

Cosgrove, R. B., and R. T. Tsunoda (2003), Simulation of the nonlinear evolution of the sporadic-E layer instability in the nighttime midlatitude ionosphere, *J. Geophys. Res.*, *108*(A7), 1283, doi:10.1029/2002JA009728.

Cosgrove, R. B., R. T. Tsunoda, S. Fukao, and M. Yamamoto (2004), Coupling of the Perkins instability and the sporadic *E* layer instability derived from physical arguments, *J. Geophys. Res.*, *109*, A06301, doi:10.1029/2003JA010295.

Dabas, R. S., L. Singh, D. R. Lakshmi, P. Subramanyam, P. Chopra, and S. C. Garg (2003), Evolution and dynamics of equatorial plasma bubbles: Relationships to E × B drift, postsunset total electron content enhancements, and equatorial electrojet strength, *Radio Sci.*, *38*(4), 1075, doi:10.1029/2001RS002586.

Ding, F., W. Wan, B. Ning, and M. Wang (2007), Large-scale traveling ionospheric disturbances observed by GPS total electron content during the magnetic storm of 29–30 October 2003, *J. Geophys. Res.*, *112*, A06309, doi:10.1029/2006JA012013.

Earle, G. D., A. M. Musumba, and J. P. McClure (2006), A global study of nighttime midlatitude topside spread echoes, *J. Geophys. Res.*, *111*, A11306, doi:10.1029/2006JA011614.

Earle, G. D., A. M. Musumba, and S. L. Vadas (2008), Satellite-based measurements of gravity wave-induced midlatitude plasma density perturbations, *J. Geophys. Res.*, *113*, A03303, doi:10.1029/2007JA012766.

Fejer, B. G., and J. T. Emmert (2003), Low-latitude ionospheric disturbance electric field effects during the recovery phase of the 19–21 October 1998 magnetic storm, *J. Geophys. Res.*, *108*(A12), 1454, doi:10.1029/2003JA010190.

Fejer, B. G., and L. Scherliess (1997), Empirical models of storm time equatorial zonal electric fields, *J. Geophys. Res.*, *102*, 24,047–24,056, doi:10.1029/97JA02164.

Fejer, B. G., L. Scherliess, and E. R. de Paula (1999), Effects of the vertical plasma drift velocity on the generation and evolution of equatorial spread *F*, *J. Geophys. Res.*, *104*, 19,859–19,869, doi:10.1029/1999JA900271.

Fejer, B. G., J. W. Jensen, T. Kikuchi, M. A. Abdu, and J. L. Chau (2007), Equatorial ionospheric electric fields during the November 2004 magnetic storm, *J. Geophys. Res.*, *112*, A10304, doi:10.1029/2007JA012376.

Haldoupis, C., M. C. Kelley, G. C. Hussey, and S. Shalimov (2003), Role of unstable sporadic-*E* layers in the generation of midlatitude spread *F*, *J. Geophys. Res.*, *108*(A12), 1446, doi:10.1029/2003JA009956.

Huang, C.-S., C. A. Miller, and M. C. Kelley (1994), Basic properties and gravity wave initiation of the midlatitude *F* region instability, *Radio Sci.*, *29*, 395–405, doi:10.1029/93RS01669.

Huang, C.-S., J. C. Foster, and M. C. Kelley (2005), Long-duration penetration of the interplanetary electric field to the low-latitude ionosphere during the main phase of magnetic storms, *J. Geophys. Res.*, *110*, A11309, doi:10.1029/2005JA011202.

Huang, C.-S., J. C. Foster, and Y. Sahai (2007), Significant depletions of the ionospheric plasma density at middle latitudes: A possible signature of equatorial spread F bubbles near the plasmapause, *J. Geophys. Res.*, *112*, A05315, doi:10.1029/2007JA012307.

Hysell, D. L. (2000), Incoherent scatter experiments at Jicamarca using alternating codes, *Radio Sci.*, *35*, 1425–1435, doi:10.1029/2000RS002368.

Kelley, M. C., and S. Fukao (1991), Turbulent upwelling of the midlatitude ionosphere: 2. Theoretical framework, *J. Geophys. Res.*, *96*, 3747–3753, doi:10.1029/90JA02252.

Kelley, M. C., J. J. Makela, B. M. Ledvina, and P. M. Kintner (2002), Observations of equatorial spread-F from Haleakala, Hawaii, *Geophys. Res. Lett.*, *29*(20), 2003, doi:10.1029/2002GL015509.

Kelley, M. C., C. Haldoupis, M. J. Nicolls, J. J. Makela, A. Belehaki, S. Shalimov, and V. K. Wong (2003), Case studies of coupling between the *E* and *F* regions during unstable sporadic-*E* conditions, *J. Geophys. Res.*, *108*(A12), 1447, doi:10.1029/2003JA009955.

Keskinen, M. J., S. L. Ossakow, and P. K. Chaturvedi (1980), Preliminary report of numerical simulations of intermediate-wavelength collisional Rayleigh-Taylor Instability in equatorial spread *F*, *J. Geophys. Res.*, *85*, 1775–1778, doi:10.1029/JA085iA04p01775.

Kil, H., L. J. Paxton, S.-Y. Su, Y. Zhang, and H. Yeh (2006), Characteristics of the storm-induced big bubbles (SIBBs), *J. Geophys. Res.*, *111*, A10308, doi:10.1029/2006JA011743.

King, G. A. (1970), Spread F on ionograms, *J. Atmos. Terr. Phys.*, *32*, 209–221, doi:10.1016/0021-9169(70)90192-3.

Lee, C.-C., J.-Y. Liu, M.-Q. Chen, S.-Y. Su, H.-C. Yeh, and K. Nozaki (2004), Observation and model comparisons of the traveling atmospheric disturbances over the western Pacific region during the 6–7 April 2000 magnetic storm, *J. Geophys. Res.*, *109*, A09309, doi:10.1029/2003JA010267.

Lee, C. C., J. Y. Liu, B. W. Reinisch, W. S. Chen, and F. D. Chu (2005a), The effects of the pre-reversal ExB drift, the EIA asymmetry, and magnetic activity on the equatorial spread F during solar maximum, *Ann. Geophys.*, *23*, 745–751.

Lee, C. C., S. Y. Su, and B. W. Reinisch (2005b), Concurrent study of bottomside spread F and bubble in the equatorial ionosphere during solar maximum using Digisonde and ROCSAT-1, *Ann. Geophys.*, *23*, 3473–3480.

Lee, J. J., K. W. Min, V. P. Kim, V. V. Hegai, K.-I. Oyama, F. J. Rich, and J. Kim (2002), Large density depletions in the nighttime upper ionosphere during the magnetic storm of July 15, 2000, *Geophys. Res. Lett.*, *29*(3), 1032, doi:10.1029/2001GL013991.

Lei, J., A. G. Burns, T. Tsugawa, W. Wang, S. C. Solomon, and M. Wiltberger (2008), Observations and simulations of quasiperiodic ionospheric oscillations and large-scale traveling ionospheric disturbances during the December 2006 geomagnetic storm, *J. Geophys. Res.*, *113*, A06310, doi:10.1029/2008JA013090.

Li, G., B. Ning, B. Zhao, L. Liu, J. Y. Liu, and K. Yumoto (2008), Effects of geomagnetic storm on GPS ionospheric scintillations at Sanya, *J. Atmos. Sol. Terr. Phys.*, *70*, 1034–1045, doi:10.1016/j.jastp.2008.01.003.

Liu, L., X. Luan, W. Wan, B. Ning, and J. Lei (2003), A new approach to the derivation of dynamic information from ionosonde measurements, *Ann. Geophys.*, *21*, 2185–2191.

Liu, L., W. Wan, C. C. Lee, B. Ning, and J. Y. Liu (2004), The low latitude ionospheric effects of the April 2000 magnetic storm near the longitude 120E, *Earth Planets Space*, *56*, 607–612.

Ma, G., and T. Maruyama (2006), A super bubble detected by dense GPS network at east Asian longitudes, *Geophys. Res. Lett.*, *33*, L21103, doi:10.1029/2006GL027512.

Martinis, C. R., M. J. Mendillo, and J. Aarons (2005), Toward a synthesis of equatorial spread F onset and suppression during geomagnetic storms, *J. Geophys. Res.*, *110*, A07306, doi:10.1029/2003JA010362.

Maruyama, T. (2006), Extreme enhancement in total electron content after sunset on 8 November 2004 and its connection with storm enhanced density, *Geophys. Res. Lett.*, *33*, L20111, doi:10.1029/2006GL027367.

McNamara, L. F., D. L. Cooke, C. E. Valladares, and B. W. Reinisch (2007), Comparison of CHAMP and Digisonde plasma frequencies at Jicamarca, Peru, *Radio Sci.*, *42*, RS2005, doi:10.1029/2006RS003491.

Miller, C. A. (1997), Electrodynamics of midlatitude spread *F*: 2. A new theory of gravity wave electric fields, *J. Geophys. Res.*, *102*, 11,533–11,538, doi:10.1029/96JA03840.

Nishioka, M., A. Saito, and T. Tsugawa (2008), Occurrence characteristics of plasma bubble derived from global ground-based GPS receiver networks, *J. Geophys. Res.*, *113*, A05301, doi:10.1029/2007JA012605.

Oyekola, O. S. (2006), Comparison between nighttime ionosonde, incoherent scatter radar, AE-E satellite, and HF Doppler observations of *F* region vertical electrodynamic plasma drifts in the vicinity of the magnetic equator, *J. Geophys. Res.*, *111*, A11318, doi:10.1029/2006JA011844.

Oyekola, O. S., and C. O. Oluwafemi (2008), Solar and geomagnetic trends of equatorial evening and nighttime *F* region vertical ion drifts, *J. Geophys. Res.*, *113*, A12318, doi:10.1029/2008JA013315.

Oyekola, O. S., A. Ojo, and J. Akinrimisi (2008), A comparison of ground and satellite observations of *F* region vertical velocity near the dip equator, *Radio Sci.*, *43*, RS1005, doi:10.1029/2007RS003699.

Perkins, F. (1973), Spread *F* and ionospheric currents, *J. Geophys. Res.*, *78*, 218–226, doi:10.1029/JA078i001p00218.

Pi, X., A. J. Mannucci, U. J. Lindqwister, and C. M. Ho (1997), Monitoring of global ionospheric irregularities using the worldwide GPS network, *Geophys. Res. Lett.*, *24*, 2283–2286, doi:10.1029/97GL02273.

Pirog, O. M., N. M. Polekh, S. V. Voeykov, G. A. Zherebtsov, and P. V. Tatarinov (2007), Ionospheric disturbances in the east Asian region during geomagnetic storm in November 2004, *Adv. Space Res.*, *39*, 1335–1341, doi:10.1016/j.asr.2007.01.017.

Rama Rao, P. V. S., P. T. Jayachandran, and P. S. Ram (1997), Ionospheric irregularities: The role of the equatorial ionization anomaly, *Radio Sci.*, *32*, 1551–1557, doi:10.1029/97RS00665.

Rich, F. J., and M. Hairston (1994), Large-scale convection patterns observed by DMSP, *J. Geophys. Res.*, *99*, 3827–3844, doi:10.1029/93JA03296.

Rodrigues, F. S., E. R. de Paula, M. A. Abdu, A. C. Jardim, K. N. Iyer, P. M. Kintner, and D. L. Hysell (2004), Equatorial spread *F* irregularity characteristics over São Luís, Brazil, using VHF radar and GPS scintillation techniques, *Radio Sci.*, *39*, RS1S31, doi:10.1029/2002RS002826.

Sahai, Y., J. Aarons, M. Mendillo, J. Baumgardner, J. A. Bittencourt, and H. Takahashi (1994), OI 630 nm imaging observations of the equatorial plasma depletions at 16°S dip latitude, *J. Atmos. Terr. Phys.*, *56*, 1461–1475, doi:10.1016/0021-9169(94)90113-9.

Sahai, Y., K. Shiokawa, Y. Otsuka, C. Ihara, T. Ogawa, K. Igarashi, S. Miyazaki, and A. Saito (2001), Imaging observations of midlatitude ionospheric disturbances during the geomagnetic storm of February 12, 2000, *J. Geophys. Res.*, *106*, 24,481–24,492, doi:10.1029/2000JA900169.

Sahai, Y., et al. (2009a), Effects observed in the Latin American sector ionospheric *F* region during the intense geomagnetic disturbances in the early part of November 2004, *J. Geophys. Res.*, *114*, A00A19, doi:10.1029/2007JA013007.

Sahai, Y., et al. (2009b), Effects observed in the ionospheric *F* region in the east Asian sector during the intense geomagnetic disturbances in the early part of November 2004, *J. Geophys. Res.*, *114*, A00A18, doi:10.1029/2008JA013053.

Saito, A., T. Iyemori, and M. Takeda (1998), Evolutionary process of 10 kilometer scale irregularities in the nighttime midlatitude ionosphere, *J. Geophys. Res.*, *103*, 3993–4000, doi:10.1029/97JA02517.

Schunk, R. W., and J. J. Sojka (1996), Ionosphere-thermosphere space weather issues, *J. Atmos. Terr. Phys.*, *58*, 1527–1574, doi:10.1016/0021-9169(96)00029-3.

Stolle, C., H. Lühr, M. Rother, and G. Balasis (2006), Magnetic signatures of equatorial spread *F* as observed by the CHAMP satellite, *J. Geophys. Res.*, *111*, A02304, doi:10.1029/2005JA011184.

Su, S.-Y., H. C. Yeh, C. K. Chao, and R. A. Heelis (2002), Observation of a large density dropout across the magnetic field at 600 km altitude during the 6–7 April 2000 magnetic storm, *J. Geophys. Res.*, *107*(A11), 1404, doi:10.1029/2001JA007552.

Su, S.-Y., C. H. Liu, H. H. Ho, and C. K. Chao (2006), Distribution characteristics of topside ionospheric density irregularities: Equatorial versus midlatitude regions, *J. Geophys. Res.*, *111*, A06305, doi:10.1029/2005JA011330.

Sultan, P. J. (1996), Linear theory and modeling of the Rayleigh-Taylor instability leading to the occurrence of equatorial spread *F*, *J. Geophys. Res.*, *101*, 26,875–26,891, doi:10.1029/96JA00682.

Tsunoda, R. T., and R. B. Cosgrove (2001), Coupled electrodynamics in the nighttime midlatitude ionosphere, *Geophys. Res. Lett.*, *28*, 4171–4174, doi:10.1029/2001GL013245.

Tsunoda, R. T., R. B. Cosgrove, and T. Ogawa (2004), Azimuth-dependent E_s layer instability: A missing link found, *J. Geophys. Res.*, *109*, A12303, doi:10.1029/2004JA010597.

Tulasi Ram, S., P. V. S. Rama Rao, D. S. V. V. D. Prasad, K. Niranjan, S. Gopi Krishna, R. Sridharan, and S. Ravindran (2008), Local time dependent response of postsunset ESF during geomagnetic storms, *J. Geophys. Res.*, *113*, A07310, doi:10.1029/2007JA012922.

Van Dierendonck, A. J., Q. Hua, and J. Klobuchar (1993), Ionospheric scintillation monitoring using commercial single-frequency C/A code receivers, paper presented at ION GPS 93, Sixth International Technical Meeting of The Satellite Division of the Institute of Navigation, Inst. of Navig., Salt Lake City, Utah, 22–24 Sept.

Wei, Y., M. Hong, W. Wan, A. Du, J. Lei, B. Zhao, W. Wang, Z. Ren, and X. Yue (2008), Unusually long lasting multiple penetration of interplanetary electric field to equatorial ionosphere under oscillating IMF B_z, *Geophys. Res. Lett.*, *35*, L02102, doi:10.1029/2007GL032305.

Woodman, R. F., and C. LaHoz (1976), Radar observations of *F* region equatorial irregularities, *J. Geophys. Res.*, *81*, 5447–5466, doi:10.1029/JA081i031p05447.

Xiao, Z., S. Xiao, Y. Hao, and D. Zhang (2007), Morphological features of ionospheric response to typhoon, *J. Geophys. Res.*, *112*, A04304, doi:10.1029/2006JA011671.

Xu, J. S., J. Zhu, and L. Li (2007), Effects of a major storm on GPS amplitude scintillations and phase fluctuations at Wuhan in China, *Adv. Space Res.*, *39*, 1318–1324, doi:10.1016/j.asr.2007.03.004.

Yeh, K. C., and C. H. Liu (1974), Acoustic-gravity waves in the upper atmosphere, *Rev. Geophys.*, *12*, 193–216, doi:10.1029/RG012i002p00193.

Yeh, K. C., and C. H. Liu (1982), Radio wave scintillation in the ionosphere, *Proc. IEEE*, *70*, 324–360, doi:10.1109/PROC.1982.12313.

Yokoyama, T., Y. Otsuka, T. Ogawa, M. Yamamoto, and D. L. Hysell (2008), First three-dimensional simulation of the Perkins instability in the nighttime midlatitude ionosphere, *Geophys. Res. Lett.*, *35*, L03101, doi:10.1029/2007GL032496.

Zhao, B., et al. (2008), Ionosphere disturbances observed throughout Southeast Asia of the superstorm of 20–22 November 2003, *J. Geophys. Res.*, *113*, A00A04, doi:10.1029/2008JA013054.

F. Ding, G. Li, L. Liu, B. Ning, W. Wan, and B. Zhao, Beijing National Observatory of Space Environment, Institute of Geology and Geophysics, Chinese Academy of Sciences, Beijing 100029, China. (dingf@mail.iggcas.ac.cn; gzlee@mail.iggcas.ac.cn; lliu@mail.iggcas.ac.cn; nbq@mail.iggcas.ac.cn; wanw@mail.iggcas.ac.cn; zbqjz@mail.iggcas.ac.cn)

J. Y. Liu, Institute of Space Science, National Central University, 300 Jungda Road, Chung-Li 32001, Taiwan. (jyliu@jupiter.ss.ncu.edu.tw)

J. S. Xu, School of Electronic Information, Wuhan University, Wuhan 430079, China. (jsxu@whu.edu.cn)

K. Yumoto, Space Environment Research Center, Graduate School of Sciences, Kyushu University, 6-10-1 Hakozaki Higashiku, Fukuoka 812-8581, Japan. (yumoto@serc.kyushu-u.ac.jp)